Frontiers in Engineering
ISSN Print: 3104-4298
ISSN Online: 3104-4301
CD ISSN: 3104-431X
https://doi.org/10.63313/FE.2012

Research on Staged Calibration of Single Injection Mass of Marine Fuel Injectors Based on Error Separation

Fengming Zhao[1]. Yipeng Sang[1]. Jinliang Zhang[1,*]. Guozhu Ren[1] and Chenguang Wang[2]
[1]Maritime College, Tianjin University of Technology, Tianjin, China
[2]Safety and Technical of industrial Products Center, Tianjin Customs District, Tianjin, China
*Corresponding Author: Jinliang Zhang

How to cite this paper: Zhao, F., Sang, Y., Zhang, J., Ren, G., & Wang, C. (2026). Research on staged calibration of single injection mass of marine fuel injectors based on error separation. Frontiers in Engineering, 2(2), 126–140. ISSN Print: 3104-4298, ISSN Online: 3104-4301.
https://doi.org/10.63313/FE.2012
Published: 2026-11-26

Copyright © 2026 by author(s) and Erytis Publishing Limited.
This work is licensed under the Creative Commons Attribution International License (CC BY 4.0).
http://creativecommons.org/licenses/by/4.0/
CC BY 4.0

Abstract

This study takes the system-level model of a 0.3 mm single-hole high-pressure common-rail injector as its object and, using the fuel injection quantity data from earlier experiments of the research group (injection pressure 35~140 MPa, Injection duration 700~3000 μs), proposes a staged calibration method based on error separation: first, grid independence verification of the number of high-pressure pipe nodes is completed and a parameter set is selected; 20 validation operating conditions are reserved from the samples and excluded from the fitting process, while the remaining conditions are used as optimization operating conditions for calibration; finally, the optimized model is selected for a full-map summary. After calibration, the mean absolute error over the 50 operating conditions decreases from 31.59% to 2.59%, and the maximum absolute error decreases from 57.58% to 9.54%.

Keywords

Marine Injector; Injection Mass; Parameter; Staged Calibration; Amesim

Introduction

Fuel injection quantity is the key link between the injection system and the combustion system. Against the backdrop of greenhouse gas emission limits, developing more efficient and cleaner combustion systems is an urgent problem in the field of marine power plants. Accurate prediction of the fuel injection quantity and injection characteristics of an injector is the foundation for the application of new fuels and emerging combustion technologies [1,2]. Compared with conventional experiments and computational fluid dynamics simulations, one-dimensional models can meet the accuracy required by engineering while substantially saving computational resources and computation time.

Amesim can represent the pressure propagation process in high-pressure circuits

and is widely used for the modeling and simulation analysis of hydraulic and injection systems [3-7]. Yang Jintao [3] established a one-dimensional model of a marine injector in Amesim and investigated the injection characteristics of the injector under high-temperature conditions. Wei Yunpeng[4] used Amesim to build an injector model that accounts for the coupling between fuel supply characteristics and injection characteristics and, on this basis, revealed the mechanism by which fuel supply characteristics, pressure accumulation characteristics and injection characteristics affect the dynamic injection characteristics of the injection system. Yang Jintao et al.[5] determined the baseline values of some structural parameters of the injector during Amesim modeling and clarified the influence trend of these parameters on fuel injection quantity. Dai Weiye et al.[6] analyzed the motion states of the solenoid valve and the needle valve and found that the inertial collision of the solenoid valve caused by unreasonable parameter settings degrades the monotonicity and stability of fuel injection quantity. Zhao Jianhui et al.[7] developed a data-driven prediction model and identified the influence of the injection interval between pilot injection and main injection on the injected mass in the main injection stage. Key parameters that determine the injection characteristics of the injector model, such as the nozzle-hole discharge coefficient, cavitation parameter and connecting volume, are often not directly accessible. However, these parameters are usually determined by repeated trial and error against experimental values[3,7,8]. It should be noted that the total error between simulated and measured fuel injection quantity does not arise entirely from model parameters; for example, the number of high-pressure pipe nodes also affects the simulation results. Therefore, error separation should be completed before calibrating model parameters, and the optimal number of high-pressure pipe nodes should be determined by grid independence verification. Few existing studies have separately evaluated the discretization error caused by differences in the number of high-pressure pipe nodes. In addition, the absence of reserved validation operating conditions during model calibration readily leads to overfitting.

To address the above problems, this study builds a one-dimensional simulation model of a marine injector based on experimental data and verifies model validity, providing a method and support for subsequent research on injection characteristics and for injector model calibration. First, a one-dimensional simulation model of a marine single-hole injector is built in Amesim. Second, the influence of the number of high-pressure pipe grid nodes on the simulation results for different injection operating conditions is discussed, and the optimal number of high-pressure pipe grid nodes is selected. Then, a parameter survey is used to determine the influence trend of all model parameters on the simulation results, and the sensitive parameters of the model are identified. Finally, a highly accurate and valid injector model is obtained by a two-stage search combined with out-of-sample validation. This study not only clarifies the sensitive parameters of the

one-dimensional injector simulation model but also provides methodological support for efficiently obtaining a highly valid injector simulation model.

1. Experimental Methods and Results

The experimental setup consists of a fuel supply system, an injection control module, the injector and its fixture, and a metering device. A commercial Bosch multi-hole injector was first modified into a single-hole injector with a large nozzle-hole diameter. The needle valve structure and cone angle of the single-hole nozzle were kept identical to those of the original multi-hole nozzle, and the machining error of the nozzle-hole diameter was less than 0.02 mm. During measurement, the nozzle hole was connected to a sealed buffer vessel, and the mass increment was measured with an FA1204B electronic analytical balance. For each operating condition, 50 consecutive injections were averaged; the test was repeated three times and the results were averaged again. The experimental setup and results are shown in Fig.1 and Table1, respectively. In Table1 the unit of Injection duration is μs, the unit of injected mass is mg, and the unit of injection pressure is MPa. Diesel was used as the test fuel, and the fuel temperature was maintained at 300 K ± 2 K during the tests. The injection pressures were 35 MPa, 50 MPa, 70 MPa, 100 MPa and 140 MPa, with a steady-state pressure error of the high-pressure rail of less than 0.5 MPa. The Injection duration ranged from 700 μs to 3000 μs, with an error of less than 50 μs. The ambient temperature was 295 K to 305 K and the ambient relative humidity was about 60%. Table1 gives the standard deviation of the three repeated measurements for each operating condition. For the 50 operating conditions within 700~3000 μs and 35~140 MPa used in this study, the median standard deviation was 0.59% and the mean was 0.88%; the standard deviation was below 1% for 36 operating conditions and below 2% for 44 operating conditions, with a maximum of 4.79%, indicating that the experiment is reliable and can be used as the calibration object for simulation calibration.

Table 1. Single-shot injected mass and standard deviation under different injection conditions

Injection duration	Injection pressure									
	35		50		70		100		140	
	Mass	Standard deviation	Mass	Standard deviation	Mass	Standard deviation	Mass	Standard deviation	Mass	Standard deviation
700	5.197	0.022	8.1625	0.057	11.512	0.127	15.390	0.215	18.762	0.062
900	9.175	0.170	13.220	0.330	15.805	0.175	18.702	0.092	21.100	0.080
1200	13.165	0.097	15.730	0.210	19.310	0.110	22.960	0.170	26.400	0.330
1500	16.197	0.042	19.510	0.410	23.215	0.255	27.800	0.080	31.965	0.085
1700	17.225	0.825	21.875	0.095	25.895	0.115	30.685	0.215	36.270	0.240
2000	20.940	0.010	25.245	0.045	29.540	0.190	34.315	1.135	41.990	1.350
2200	22.760	0.030	27.495	0.035	32.340	0.020	38.355	0.155	44.630	0.100
2500	25.155	0.235	30.785	0.115	36.085	0.105	43.180	0.060	50.505	0.355
2700	27.450	0.330	32.915	0.295	38.815	0.235	46.085	0.075	53.340	0.250
3000	30.150	0.070	35.395	0.865	42.575	0.295	50.585	0.265	58.550	0.120

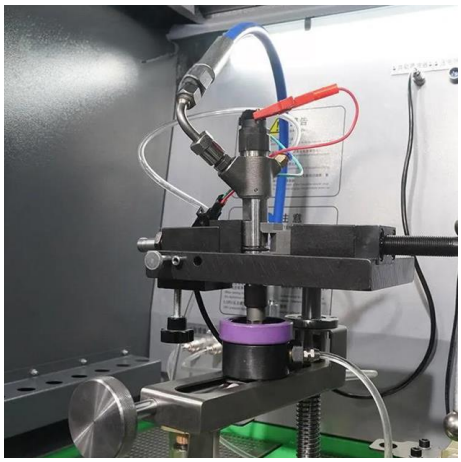

Fig 1. Experimental setup of the injector

2. Model Development and Validation

2.1. Model Development

In this study, a single-hole injector model is built in Simcenter Amesim. The model takes the high-pressure rail as the pressure boundary, which is connected to the injector inlet through the high-pressure pipe and the fuel inlet pipe. The injector consists of a control chamber, inlet and outlet damping orifices, a ball valve, a control plunger, a needle valve~spring assembly, a nozzle pressure chamber and nozzle holes. The solenoid valve is driven by the signal and control library, with injection pressure and Injection duration as inputs and single-shot fuel injection quantity as output. The high-pressure pipe and the fuel inlet pipe adopt a one-dimensional CFD pipe submodel to describe pressure wave propagation. The rail, control chamber and nozzle pressure chamber adopt lumped-volume or variable-volume submodels. The needle valve, control plunger and ball valve adopt a mass~spring~damper mechanical submodel. The damping orifices and the nozzle hole adopt a variable-orifice submodel, with a discharge coefficient and a cavitation parameter introduced to characterize throttling losses. The simulation model parameters come from drawing design values and empirical values. The simulation model contains 396 configurable parameters in total, of which 284 are modifiable variable parameters and 112 are switch parameters. The simulation model and geometric structure of the injector are shown in Fig.2.

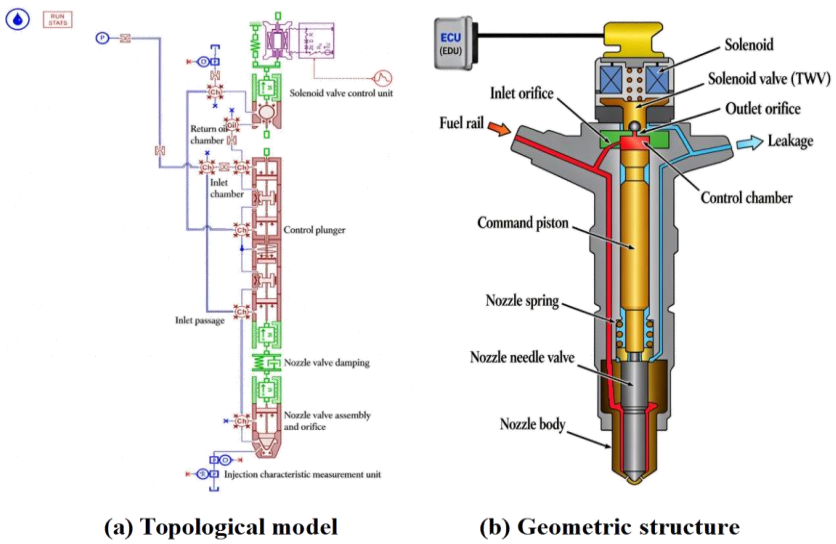

Fig 2. Simulation model and geometric structure of the injector

2.2. Grid Independence Verification

In the simulation model, the high-pressure line adopts a one-dimensional CFD pipe submodel, and the high-pressure pipe is spatially discretized into a number of segments; the number of segments is a numerical setting of the model rather than a physical parameter. The number of discrete nodes of the high-pressure pipe affects both the model results and the computation time. The number of high-pressure pipe nodes was increased from 8 to 1024, while the remaining simulation duration, fluid properties, boundary conditions, and the parameters and numerical settings of the other components were kept unchanged. Taking an injection pressure of 140 MPa and Injection duration of 700 μs, 1500 μs, 2200 μs and 3000 μs as examples, the influence of the number of high-pressure pipe nodes on the calculation results is shown in Fig.3. As the number of high-pressure pipe nodes increases from 8 to 1024, the injected mass increases for all experimental operating conditions, and the longer the Injection duration, the smaller the influence of the number of nodes on injected mass. For Injection duration of 3000 μs, 2200 μs, 1500 μs and 700 μs, the injected mass increases by 4.58%, 7.72%, 9.63% and 13.87%, respectively. Since a larger number of nodes gives the most accurate simulation of the final fuel injection quantity, 1024 nodes is taken as the reference; the other node levels are evaluated by simulation and their residual deviation is calculated as shown in Eq. (1):

$$\delta_{N,j}=\left|\frac{m_{N,j}-m_{1024,j}}{m_{1024,j}}\right|\times 100\% \quad (1)$$

In Eq. (1), $m_{N,j}$ denotes the simulated fuel injection quantity of the j-th operating condition when the high-pressure pipe uses N nodes; $m_{1024,j}$ denotes the

simulated fuel injection quantity of the same operating condition when the high-pressure pipe uses 1024 nodes; and $\delta_{N,j}$ denotes the residual deviation of the N-th grid relative to the 1024-node grid; j = 700, 1500, 2200, and 3000 μs, all at 140 MPa.

Convergence is considered to be achieved when the residual deviation after increasing the number of nodes is less than 1.5%. The influence of the number of high-pressure pipe nodes on the residual deviation is shown in Fig.3(b). The residual deviation is inversely proportional to the number of nodes, and the residual deviation of all operating conditions converges when the number of nodes increases to 256. Table2 lists the computation time for all operating conditions with different numbers of high-pressure pipe nodes. As the number of nodes increases, the decline of the residual deviation slows down while the simulation cost increases. When the number of high-pressure pipe nodes increases from 256 to 512, the average computation time rises sharply, and the residual deviation has already converged at 256 nodes. Therefore, the number of high-pressure pipe nodes is set to 256 for all simulation operating conditions in this study.

Table 2. Simulation time for different numbers of high-pressure pipe nodes

Injection duration	Number of high-pressure pipe nodes							
	8	16	32	64	128	256	512	1024
700μs	9.7	10.8	14.1	20.0	32.4	55.9	118.3	316.9
1500μs	7.7	9.5	13.2	21.1	37.8	67.9	130.5	313.7
2200μs	7.4	9.4	13.2	20.7	32.5	59.4	125.5	327.7
3000μs	7.3	9.5	13.3	20.6	33.3	59.7	124.1	326.7
Average computation time	8.0	9.8	13.5	20.6	34.0	60.7	124.6	321.3

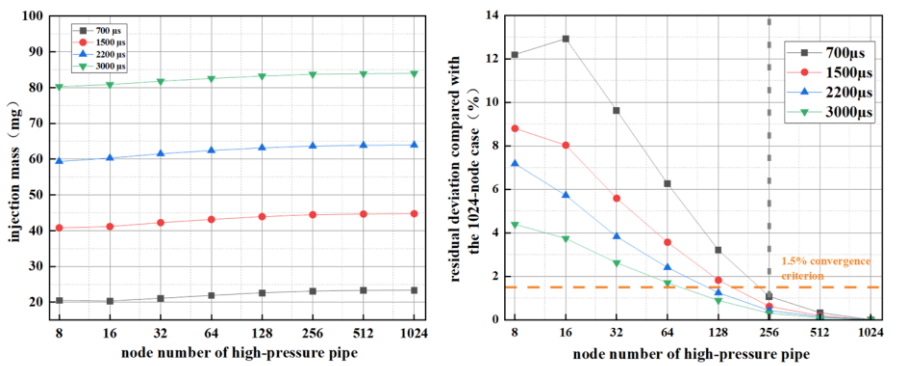

（a）Change in injected fuel quantity versus node number （b）Residual error relative to the 1024-node number case

Fig 3. Influence of the number of nodes on simulation results

2.3. Model Validation

After the confirmable parameters were modified according to the experimental operating conditions, the remaining parameters were set to the system default values for simulation. The comparison between the simulated and experimental single-shot injected mass is shown in Fig.4. The simulated fuel injection quantity differs considerably from the experimental value for each operating condition, and

the deviation between simulation and experiment generally exceeds 30%. The higher the injection pressure and the longer the Injection duration, the larger the deviation between the simulated and experimental values. The model validation results show that the deviation between the injector model built with default parameters and the actual situation exceeds the engineering allowable range, so injection research cannot be carried out with the default parameters

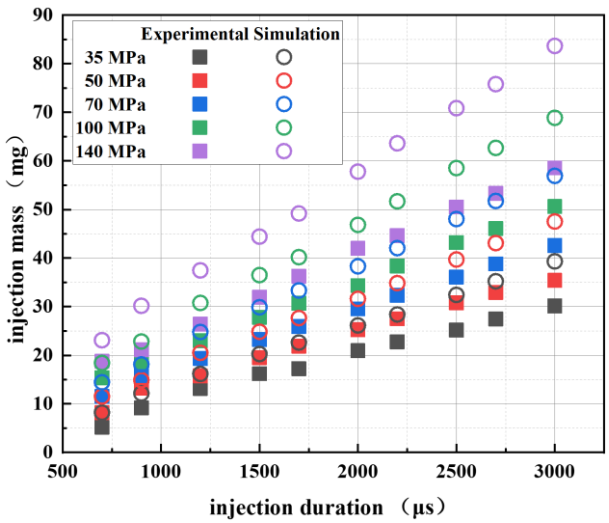

Fig 4. Model validation

3. Optimization Method

As mentioned above, model calibration using default model parameters and empirical parameters suffers from insufficient accuracy and low efficiency, and calibrating a model by parameter trial and error is extremely time-consuming. To improve the efficiency and accuracy of model calibration, this paper proposes a method that combines a two-stage search based on a parameter survey and prior constraints with out-of-sample validation, so as to improve the efficiency and accuracy of injector model calibration. The workflow of parameter optimization and model calibration is shown in Fig.5.

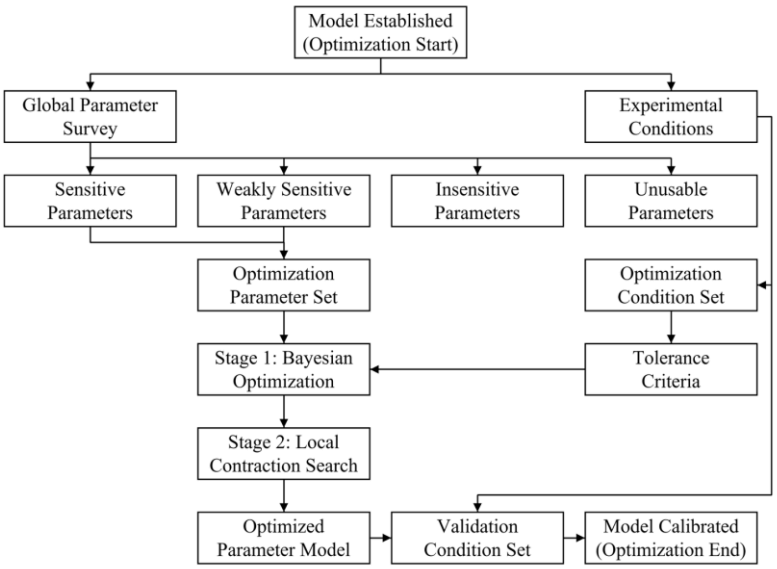

Fig 5. Model calibration method and workflow

3.1. Model Parameters

The one-dimensional injector model built in Amesim contains 396 modifiable parameters, including 283 continuous parameters, 112 switch parameters and the number of high-pressure pipe nodes. The 283 adjustable parameters were assigned values of 0.70, 0.85, 1.00, 1.15 and 1.30 times their system default values; a value exceeding the physical constraints was excluded from the simulation. The influence of the adjustable parameters on the injected mass of the model was analyzed for five experimental operating conditions: Injection duration 700 μs with injection pressure 35 MPa; 700 μs with 70 MPa; 900 μs with 100 MPa; 1200 μs with 140 MPa; and 3000 μs with 50 MPa. An adjustable parameter whose influence on injected mass exceeds 5% is defined as a sensitive parameter; one below 1% is defined as a stable parameter; one with an influence magnitude between 1% and 5% is defined as a weakly sensitive parameter; and one that causes model divergence is defined as an unusable parameter. The influence magnitude of all adjustable parameters on injected mass is shown in Fig.6. The results show that the adjustable parameters include 43 sensitive parameters, 15 weakly sensitive parameters, 6 unusable parameters and 219 insensitive parameters. All 6 unusable parameters are related to mechanical friction; any non-zero value of these parameters causes model divergence. Table3 lists the 8 sensitive parameters with the largest influence magnitude and their influence trends on injected mass. As shown in Table3, the parameters with the most significant influence on injected mass are mainly concentrated in the moving parts of the needle valve and plunger and in the opening and closing parameters of the nozzle, and their influence on injected mass shows no obvious regularity. A total of 58 adjustable parameters, comprising the sensitive and

weakly sensitive parameters, are selected as the parameter calibration set for the subsequent optimization and calibration process.

Table 3. Eight sensitive parameters with significant influence

No.	Parameter	Influence magnitude (%)	Influence trend
1	Control plunger diameter	8014	Non-monotonic
2	Lower piston diameter of needle valve spring	8011	Non-monotonic
3	Front piston diameter	7983	Non-monotonic
4	Lower piston rod diameter	7973	Decreases then increases
5	Ball valve zero-position lift	7909	Monotonically increasing
6	Nozzle seat under lap	4865	Monotonically increasing
7	Minimum nozzle opening	4202	Monotonically increasing
8	Minimum ball valve opening	2137	Monotonically increasing

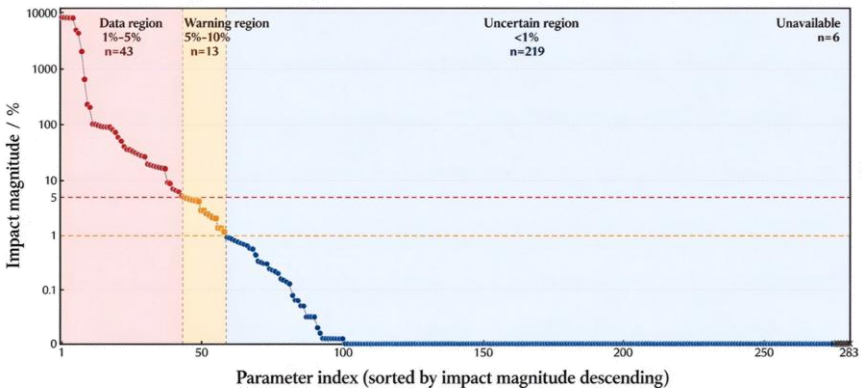

Fig 6. Results of the global parameter survey of the model

3.2. Evaluation Criteria

3.2.1. Tolerance Contract

A large number of experimental and simulation studies have shown that the stability of injected mass deteriorates under both short and long Injection duration[1,9]. Therefore, in this study the errors between simulated and experimental values under different Injection duration are classified according to the stability of injected mass, as shown in Table4. Injection duration of 700 μs and 3000 μs are assigned to the high-tolerance interval, and the operating conditions with Injection duration from 900 μs to 2700 μs are assigned to the low-tolerance interval. Within the high-tolerance and low-tolerance intervals, the maximum error between experimental and simulation results should be less than 10% and 5%, respectively. The number of operating points in the high-tolerance interval accounts for 20% of all experimental operating conditions. The maximum error value is kept unchanged during adjustable parameter optimization and model validation.

Table 4. Tolerance intervals and maximum errors

Interval	**Injection duration / μs**	**Number of operating conditions**	**Maximum error**
Low-tolerance interval	900~2700	40	≤5%

High-tolerance interval	700、3000	10	≤10%

3.2.2. Selection of Optimization and Validation Operating Conditions

Validation operating points are reserved before parameter optimization to prevent overfitting during model calibration. Validation operating points do not participate in optimization or calibration; they are used only to verify and check the model and the optimized parameters after the adjustable parameters have been optimized. To ensure both the quality of parameter optimization and the optimization time, 30 operating points are selected as the optimization set and 20 operating points as the validation set. The injection pressures and Injection duration corresponding to the optimization set Y and the validation set C are shown in Table5. The validation set covers all injection pressures and Injection duration.

Table 5. Validation and optimization operating points

Injection pressure	Injection duration									
	700	900	1200	1500	1700	2000	2200	2500	2700	3000
35	C	Y	Y	Y	C	Y	Y	Y	C	C
50	Y	Y	C	C	Y	Y	C	C	Y	Y
70	Y	C	Y	Y	C	C	Y	Y	C	Y
100	Y	Y	C	C	Y	Y	C	C	Y	Y
140	C	C	Y	Y	Y	C	Y	Y	Y	C

3.2.3. Objective Function

The objective function for parameter optimization consists of five components, all evaluated on the optimization set:

$$J(u)=\frac{1}{N_a}\sum_{i=1}^{N_a}|e_i(u)|+\frac{3}{N_{mid}}\sum_{i\in A_{mid}}\max(0,|e_i|-0.05)+\frac{1}{N_{end}}\sum_{i\in A_{end}}\max(0,|e_i|-0.10)+\frac{\lambda_p}{d}\sum_{j=1}^{d}u_j^2+0.5\frac{n_{fail}}{N_a} \quad (2)$$

In Eq. (2), $\frac{1}{N_a}\sum_{i=1}^{N_a}|e_i(u)|$ is the mean relative error over the optimization operating conditions. Optimization operating conditions with solution failure are counted as 100% in this term. $\frac{3}{N_{mid}}\sum_{i\in A_{mid}}max(0,|e_i|-0.05)$ is the average portion exceeding 5% for the middle-range optimization operating conditions with Injection duration of 900–2700 μs; operating conditions that do not exceed the limit contribute 0, and the coefficient 3.0 is the weight of this term. $\frac{1}{N_{end}}\sum_{i\in A_{end}}max(0,|e_i|-0.10)$ is the average portion exceeding 10% for the end optimization operating conditions with Injection duration of 700 and 3000 μs, with a weight of 1.0. $\lambda_p\cdot\frac{1}{d}\sum_{j=1}^{d}u_j^2$ is the prior penalty term. The term u_j^2 is defined according to Eq. (3), and λ_p is set to 0.02. $0.5\frac{n_{fail}}{N_a}$ is a penalty on the proportion of optimization operating conditions with solution failure, used to suppress parameter combinations that drive the model into a non-physical solution region.

The purpose of the limit-exceedance penalty term is to avoid solutions in which the average meets the target while individual operating conditions severely exceed the limit: if only the mean error is used as the objective, the optimizer can trade large positive deviations at a few operating conditions for improvements at most

conditions. In the prior penalty term, parameters participate in the search in a dimensionless form relative to their prior width, namely

$$u_j=\frac{v_j-v_j^0}{\sigma_j},u_j\in\left[u_j^L,u_j^U\right] \tag{3}$$

In Eq. (3), v_j^0 denotes the baseline parameter value, and σ_j denotes the prior width of that parameter. The prior width is assigned by parameter category: 2%–3% for measured geometry (piston and rod diameters, pipe diameters, etc.); 10%–15% for design geometry (chamber volume, lift limit, seat half-angle, etc.); 25%–40% for empirical coefficients (discharge coefficient, cavitation number, critical flow number, etc.); 15%–25% for electrical parameters; and 15%–20% for spring characteristics. The search range is limited to $|u_j| \le 2.5$.

3.2.4. Two-Stage Search

The entire two-stage search is carried out on the 30 optimization operating conditions. The first stage is the global Bayesian optimization stage: a Gaussian process surrogate model and the expected improvement (EI) acquisition function are used to evaluate 200 candidates in total, where the Gaussian process surrogate model is:

$$k(x,x')=\left(1+\frac{\sqrt{5}r}{l}+\frac{5r^2}{3l^2}\right)\exp\left(-\frac{\sqrt{5}r}{l}\right),r=\|x-x'\|_2 \tag{4}$$

In Eq. (4), x and x' denote two parameter combinations in the parameter space, and $r=\|x-x'\|_2$ is their Euclidean distance in the standardized parameter space. The length scale l characterizes how quickly the kernel correlation decays as the distance between parameter combinations increases; a larger l gives a smoother surrogate surface, while a smaller l makes the model more sensitive to local parameter changes. The expected improvement acquisition function is given in Eq. (5):

$$EI(x)=(J_{best}-\mu(x))\Phi(z)+s(x)\phi(z),z=\frac{J_{best}-\mu(x)}{s(x)} \tag{5}$$

In Eq. (5), $EI(x)$ denotes the expected improvement evaluated at the parameter combination x and measures how worthwhile further simulation at that point is. J_{best} denotes the minimum objective function value among the completed evaluations, that is, the mean absolute error of the current best parameter set on the optimization conditions. $\mu(x)$ and $s(x)$ are the predicted mean and predicted standard deviation from the Gaussian-process model in Eq. (4). $z=\frac{J_{best}-\mu(x)}{s(x)}$ is the standardized improvement, representing by how many predicted standard deviations the predicted value is better than the current best solution. $\Phi(z)$ and $\phi(z)$ are the cumulative distribution function and probability density function of the standard normal distribution, respectively; the former corresponds to the probability that an improvement occurs, and the latter to the expected magnitude of

the improvement. The sum of these two terms allows EI to strike a balance between the exploitation region with low prediction error and the exploration region with high prediction uncertainty, thus preventing the search from converging prematurely on a local optimum.

The second stage, the local contraction search stage, starts from the best solution of the first stage and uses a random search with a contracting radius: the errors of the 30 optimization operating conditions are written as a linear function of the 58 parameter displacements; the unique minimum displacement combination is solved by regularized least squares with λ, and the physical constraints are determined; after each solution step the result is rechecked by real simulation, then the residual is recomputed at the new working point and solved again, and finally the search step size of each parameter is determined. After calibration, the displacement distribution of the 58 parameters is 37 in 0∼0.5σ, 15 in 0.5∼1.0σ, 4 in 1.0∼1.5σ and 2 in 1.5∼2.0σ, with a maximum displacement of 1.98σ.

Candidate generation for the local search:

$$\Delta u_j=\rho\xi_j(j\in F),\Delta u_j=0(j\notin F),\xi_j\sim N(0,1),u_{new}=clip(u_c+\Delta u,u^L,u^U) \quad (6)$$

In Eq. (6), u_c denotes the currently retained best parameter combination and is the starting point of this round of local search. u_{new} denotes the candidate parameter generated after perturbation. ρ is the search radius, representing the perturbation amplitude of each free parameter relative to its prior width. ξ_j denotes mutually independent standard normal random numbers and provides a random perturbation direction for the j-th parameter. Δu_j is the displacement component of the j-th parameter. $\mathcal{F}$ is the index set of free parameters participating in perturbation in this round. Parameters outside this set have their displacements forced to zero, i.e. they remain fixed during the local search stage to reduce ineffective search dimensions. $clip(\cdot)$ is the truncation operator, which constrains the perturbed values to the physically feasible range of the parameters so as to avoid generating meaningless parameter combinations.

Radius contraction and acceptance criterion:

$$\rho_{k+1}=0.75\rho_k,\rho_0=0.40,\rho_{min}=0.03$$

$$u_c\leftarrow u_{new}\Leftrightarrow J(u_{new})<J(u_c)\text{ and }n_{fail}=0 \quad (7)$$

In Eq. (7), the initial search radius ρ_0 = 0.40, the termination radius ρ_{min} = 0.03, and the contraction rule $\rho_{k+1}=0.75\rho_k$ indicate that when no candidate in a batch yields an improvement, the search radius is contracted to 75% of its previous value, so that the search gradually transitions from coarse tuning to fine tuning. The local search terminates once the radius falls below the termination radius. u_c denotes the currently retained solution, and u_{new} denotes the candidate solution. $J(u_c)$ and $J(u_{new})$ are their corresponding objective function values, and n_{fail} is the number of simulation failures of the candidate solution when solving the optimization operating conditions. The retained solution is replaced by u_{new} only when $J(u_{new}) < J(u_c)$ and no failed optimization operating conditions occur;

otherwise the original solution is retained and candidates are regenerated after the radius is contracted according to the above rule, so that the solution remains feasible and monotonically non-degrading throughout the local search.

4. Results and Discussion

4.1. Validation Operating Condition Check

The objective function is built only on the 30 optimization operating conditions (Section 3.2.3); the 20 validation operating conditions other than the optimization operating conditions do not participate in fitting. The results are given in Table6. The mean absolute error of the 30 optimization operating conditions is 2.41% and the maximum absolute error is 7.63%. For the 20 pre-specified validation operating conditions, which never participated in fitting, the final model gives a mean error of 2.87% and a maximum error of 9.54%, showing no sign of overfitting.

Table 6. Out-of-Sample Validation

Data set	Number of operating conditions	Mean absolute error / %	Maximum absolute error / %	Relative error range / %
Optimization operating conditions	30	2.41	7.63	−6.05%~+7.63%
Validation operating conditions	20	2.87	9.54	−8.12%~+9.54%

4.2. Summary of Calibration Results

The model error is improved after calibration, and the error results for the different intervals are shown in Table7. The mean absolute errors of both intervals are within 5%; in the middle interval there are three out-of-limit points exceeding the required maximum error of 5%, while at the two ends there are no out-of-limit points and all values are within the required maximum error of 10%. The overall mean absolute error is reduced to below 5%, as shown in Fig.7. Fig.7(a) shows the error distribution before calibration. After the baseline model is rebuilt on the converged grid, the errors of the operating conditions are recalculated; their notable feature is that the errors of all 50 operating conditions are positive, i.e. the calculated fuel injection quantity is systematically higher than the measured value, with an error range of +12.50% to +57.58% and a full-map mean absolute error of 31.59%.

Fig.7(b) shows the error distribution after calibration. Across the 50 full-map operating conditions the mean is 2.59% and the maximum is 9.54%, with all 50/50 within 10%. For the 20 validation operating conditions that never participated in fitting, the mean is 2.87% and the maximum is 9.54%, also all within 10%, with a signed mean of +0.26% (29 positive, 21 negative), indicating neither systematic bias nor overfitting.

Fig.8 compares the simulated and experimental fuel injection quantity after calibration: the simulated and experimental fuel injection quantity points closely

coincide for every operating condition, and the dashed experimental line and the solid simulation line essentially overlap, indicating that the pre-existing parameter deviation has been largely eliminated and the model meets the requirements.

Table 7. Error results for different intervals

Interval	Number of operating conditions	Mean absolute error / %	Maximum absolute error / %	Relative error range / %
Low-tolerance interval	40	2.22	6.63	−6.05%~+6.63%
High-tolerance interval	10	4.07	9.54	−8.12%~+9.54%

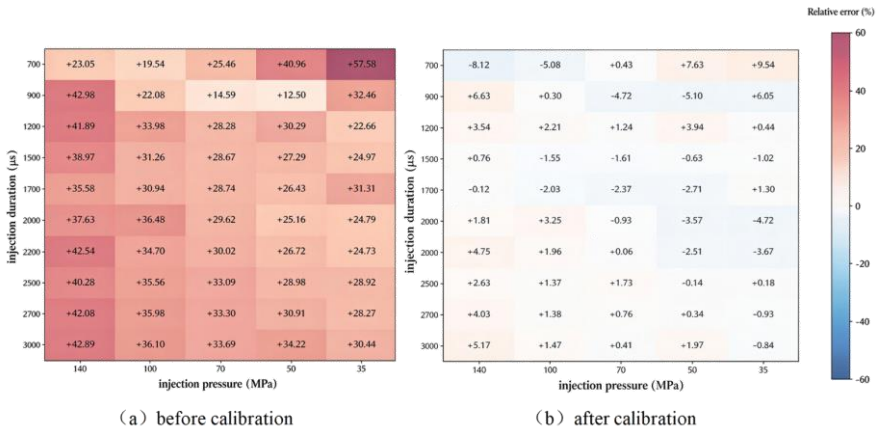

Fig 7. Calibration results

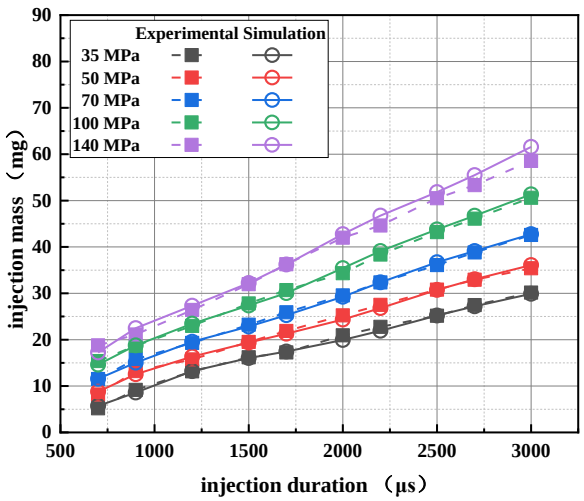

Fig 8. Analysis of calibration results

5. Conclusions

(1) A staged calibration method is proposed and validated, proceeding from grid independence verification to a global parameter survey, then to prior-constrained two-stage calibration, and finally to out-of-sample validation. It is also clarified that

without fixing the number of high-pressure pipe nodes first, the sources of error cannot be attributed.

(2) After calibration, the mean absolute error of the 50 operating conditions within the applicable range decreases from 31.59% to 2.59%, and the error changes from a one-sided positive bias (+12.5% to +57.6%) to a two-sided distribution. The low-tolerance interval meets the target with a mean of 2.22%, with three single-point exceedances and a maximum of 6.63%; all 10 points at the two ends are ≤10%, and the full-map mean of 2.59% meets the target.

(3) The mean absolute error of the validation operating conditions is 2.87%, close to the mean absolute error of 2.41% for the 30 optimization operating conditions, indicating no overfitting to the data sample; the model is qualified and the method is applicable.

(4) Scope of applicability and limitations: the conclusions are limited to this 0.3 mm single-hole injector, 700~3000 μs and 35~140 MPa, and the 256-node high-pressure pipe setting. Calibration is matched only against the integral quantity of fuel injection quantity; the residual deviations in the 700 μs and 900 μs rows are dominated by tilt and scatter and cannot be corrected by a shift, so further attribution requires measurements of internal quantities.

References

[1] Lu Xiuwei. Research on Spray and Ignition Characteristics of Heavy Oil based Blends [D]. Shanghai: Shanghai Maritime University, 2024.

[2] Wang Ziman, Yang Jinyu, Xiang Heping, et al. Working Characteristics of Common Rail Injectors in High-Heat Environment [J]. Chinese Internal Combustion Engine Engineering, 2026, 47(04): 92-101.

[3] Yang Jintao. Construction of Digital Simulation Platform for High-Pressure Common Rail Fuel System and Research on the Design and Application of Fuel Injection [D]. Harbin: Harbin Engineering University, 2025.

[4] Wei Yunpeng. Study on dynamic injection characteristics of a marine diesel high-pressure common-rail system [D]. Harbin: Harbin Engineering University, 2023.

[5] Yang Jintao, Zhang Heng, Zhao Jianhui, et al. School of Power and Energy Engineering,Harbin Engineering University Department of Piston Engines, Bauman Moscow State Technical University [J]. Journal of Harbin Engineering University, 2025, 46(02): 276-282.

[6] Dai Weiye, Wen Qin, Li Yuhe. Study on"Non-Ballistic Region"Injection Law of High Pressure Common Rail Diesel Injector [J]. Internal Combustion Engine & Parts, 2025(18): 22-24.

[7] Zhao Jianhui, Lan Zhongze, Lu Xiangdong, et al. Injection Quantity Prediction of High-Pressure Common Rail Systems under Multiple Injections Based on Gaussian Process Regression [J]. Journal of Southwest Jiaotong University, 2026, 61(02): 299-307.

[8] Pan Yan, Liu Hua, Deng Shengjiang, et al. Simulation research on the influence of structural parameters of electronic control unit pump on fuel injection characteristics [J]. Journal of Chinese Agricultural Mechanization, 2025, 46(05): 283-290.

[9] Lan Qi, Bai Yun, Fan Liyun, et al. Investigation on Dynamic Response of Electronically Controlled Injector for Low-Speed Marine Diesel Engines [J]. Chinese Internal Combustion Engine Engineering, 2020, 41(6): 55-64.